



Perylene diimide based fluorescent sensors for aqueous detection of perfluorooctane sulfonate (PFOS)

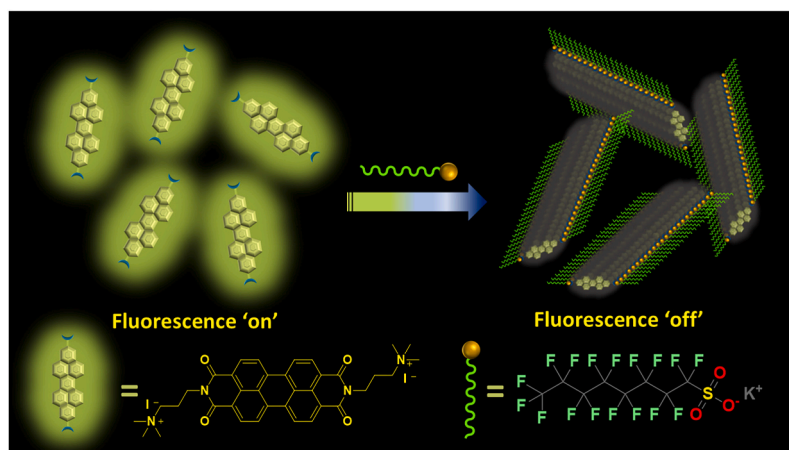
Rana Dalapati, Saravanakumar Manickam, Jiangfan Shi , Matthew Hunter, Ling Zang*

Department of Materials Science and Engineering, University of Utah, Salt Lake City, UT, 84112, USA

HIGHLIGHTS

- Novel sensor shows high sensitivity and selectivity for PFOS detection in water.
- Sensing mechanism involves supramolecular complex between fluorophore and PFOS.
- A low LOD of 3.5 nM (1.9 ppb) is ideal for onsite water monitoring.
- Design principles are extensible to creating water-soluble sensors for other PFAS.

GRAPHICAL ABSTRACT



ARTICLE INFO

Handling Editor: Prof Rebecca Lai

Keywords:

Perylene diimide
PFAS
PFOS
Fluorescent sensor
Water pollution

ABSTRACT

Background: Perfluorooctane sulfonate (PFOS), one of the most harmful members of the large group of per- and poly-fluoroalkyl substances (PFAS), is notorious for its environmental persistence, bioaccumulation, and toxic effects, raising serious environmental and health concerns. Developing rapid and sensitive methods to detect PFOS in water is critical for effective monitoring and protection against this hazardous chemical.

Results: In this study, we developed rapid and highly sensitive fluorometric sensors (**PDI-2+**, **PDI-6+**) for detecting PFOS. We also investigated the influence of the sensor's molecular structure on its performance. Our findings reveal that the formation of a supramolecular complex between PFOS and the cationic fluorophores, facilitated by the synergistic interplay of electrostatic, hydrophobic and π - π stacking interactions, enables a quick and efficient fluorometric sensing response for the detection of PFOS in aqueous systems. Remarkably, the detection limit for PFOS was found to be as low as 3.5 nM (1.9 ppb) for **PDI-2+** and 2.7 nM (1.4 ppb) for **PDI-6+**, showcasing the high sensitivity of the sensor. The PDI sensors also demonstrate a high level of selectivity for PFOS against PFOA (another top two PFAS designated as hazardous substances by the U.S. EPA), other PFAS like GenX, structurally similar detergents, and inorganic salts typically found in water. Furthermore, the sensor's successful detection of PFOS in real water samples underscores its potential for environmental monitoring.

* Corresponding author.

E-mail address: lzang@eng.utah.edu (L. Zang).

<https://doi.org/10.1016/j.aca.2025.343670>

Received 8 October 2024; Received in revised form 30 December 2024; Accepted 14 January 2025

Available online 15 January 2025

0003-2670/© 2025 Elsevier B.V. All rights are reserved, including those for text and data mining, AI training, and similar technologies.

Significance: The development of novel, water-soluble fluorometric sensors offers a promising solution for the rapid and sensitive detection of PFOS in water. Their high selectivity and low detection limits make them valuable tools for environmental monitoring and pollution control. The findings of this study contribute to the advancement of analytical techniques for PFAS detection and support ongoing efforts to mitigate the environmental and health risks posed by PFOS contamination.

1. Introduction

Per- and poly-fluoroalkyl substances (PFAS) have emerged as a class of water pollutants of global concern due to their severe and long-standing impact on the environment and public health [1–8]. These substances are often referred to as 'forever chemicals' because of their extreme persistence to degradation under normal environmental conditions. For many decades, PFAS have been broadly used in industry and consumer products, such as aqueous film-forming foam (AFFF), nonstick cookware, fast food wrappers, stain-resistant fabrics, cleaning products, and personal care products [1–3]. Extensive, long-term use has distributed PFAS in various bodies of water, including drink, ground and rain water. Among the large number of PFAS identified (currently over 9000), perfluorooctane sulfonate (PFOS) and perfluorooctanoic acid (PFOA) represent the most common species found in the environment and the most extensively studied in terms of severe health and environment impact [1,4,9–11]. While now banned in the U.S. and many other countries, PFOS and PFOA were commonly used in AFFFs, and many other products. The wide and longtime use makes the pollution caused by these two PFAS a serious global concern. As estimated by a recent study, 0.4–1 million people in the United States may receive tap water contaminated by PFOA and PFOS at concentration above the EPA advisory level of 4 ppt [12]. As evidenced in recent research, exposure to these two PFAS compounds may cause chronic kidney disease, thyroid dysfunction, and some forms of cancer [4,11,13]. Due to growing exposure and health risks, PFOS and PFOA have recently been designated by the U.S. EPA as hazardous substances under the Comprehensive Environmental Response, Compensation, and Liability Act (CERCLA), also known as Superfund [14].

In response to the growing concern over PFAS pollution, significant efforts have been made to develop detection methods capable of analyzing PFAS rapidly and accurately, aiming to identify contaminated waters and, ideally, trace the source of the contamination [11]. To comply with the U.S. EPA regulations, and as generally required for chemical detection, the new detection methods must satisfy three criteria: sensitivity, selectivity, and portability for onsite deployment.

The current detection technology for PFAS is dominated by liquid chromatography coupled with tandem mass spectrometry (LC-MS/MS) [9,11,15–17], which remains a standard as verified by the EPA as Method #1633 [18]. By coupling with a solid phase extraction (SPE) preconcentration, this method can reach a limit of detection (LOD) of 0.3 ppt for measuring PFOS and PFOA in water samples. This level of sensitivity is sufficient for detecting the PFAS pollution in drinking water, for which the official health advisory level set by the U.S. EPA for PFOA and PFOS is 4 ppt [19]. In addition to the high sensitivity (low LOD), the LC-MS/MS method also provides high specificity for identifying and quantifying different PFAS. However, LC-MS/MS requires sophisticated, expensive instruments, highly-trained personnel, tedious sample preparation, and laborious data collection processes. It remains imperative to develop new detection technologies that are not only accurate and reliable, but also portable, easy to use, and thus suitable for onsite detection [11]. Rapid, onsite monitoring of PFAS could significantly reduce the amount of time and costs needed for characterization, and would enable the detection of PFAS in real-time, and onsite at various physical locations to assess remediation or sequestration efforts.

To overcome drawbacks of the non-portable LC-MS/MS detection method, a variety of chemical sensors based on different molecules and materials have been developed and tested for quick, simple detection of

PFAS [11,16,20–26]. Generally, these sensors can be classified into two major categories according to their sensing mechanisms: optical sensors (e.g., based on colorimetric and fluorescent modulations), and electrochemical sensors. Most of the sensors were investigated with PFOS and PFOA as the target analytes. The LODs obtained for optical sensors are generally around the high ppb or even ppm level [11,15,20,27,28], which fall short of the EPA requirement for detecting PFAS in drinking water. Comparable sensing responses were also observed for other PFAS, and the fluorescence quenching was significantly affected by the presence of other surfactants like SDS, CTAB, etc. Additionally, the nanoparticle sensor can only function in organic media, like dimethylformamide, due to its poor dispersion and weak fluorescence in water [29]. This mandates extra sample pretreatment for analysis of PFAS in water samples. Electrochemical sensors, usually based on voltammetry, potentiometry or impedance spectrometry, have been well studied for trace level detection of PFAS directly in water [30–36]. By modifying the electrode with metal organic framework (MOF) or molecular imprinted polymer (MIP), the LOD reaches low ppt levels, e.g., 20 ppt for PFOS [33]. The use of a MIP template helps improve detection selectivity towards specific PFAS, though the intrinsic fragility of MIP templates and the associated complications in electrode surface modification may impact the measurement repeatability and robustness when compared to spectrometry methods. In summary, few of the chemical sensors developed to date meet the key technical criteria of sensitivity, selectivity, and repeatability. These factors are essential for enabling their practical application in monitoring PFAS in water environments.

We report herein on three novel fluorescent sensor molecules as shown in Scheme 1. The sensors, namely **PDI-2+**, **PDI-6+** and **PDI-Cl-2+**, are based on a perylene diimide (PDI) structure modified with two or six quaternary trimethylammonium cationic side groups. The sensing mechanism is based on fluorescence quenching of the PDI fluorophore. The cationic PDI fluorophores, exemplified by **PDI-2+**, demonstrate a strong green emission in water devoid of PFOS, which is a signature for the molecularly dispersed (non-aggregated) form of the fluorophore. The situation changes in the presence of PFOS, which complexes with **PDI-2+**, causing aggregation of the fluorophores as illustrated in Scheme 1. The aggregation is a result of several synergistic intermolecular interactions between PFOS and the fluorophore, including electrostatic attraction between the head groups, π - π stacking between PDI backbones, and hydrophobic association between the perfluoroalkyl chains of PFOS. In the aggregate state, the π - π stacking quenches the emission of PDI, a common phenomenon of aggregation induced quenching for π -conjugated fluorophores [37,38]. The relative decrease in emission intensity measured can be correlated to the concentration of PFOS in solution, thereby providing a calibration curve for quantitative analysis. A LOD of 1.9 ppb was obtained for **PDI-2+** and 1.4 ppb for **PDI-6+** in the detection of PFOS. By combining with the concentration power of SPE ($\sim 1000 \times$) [39], the LOD of this sensor could be pushed down to the level below 4 ppt, which is the EPA advisory level for PFOS in drinking water. In addition to high sensitivity, the two PDI sensors also demonstrate a high level of selectivity for PFOS against other PFAS (particularly PFOA, GenX) and common detergents (e.g., SDS) typically found in water.

2. Experimental section

2.1. Materials and instrumentations

All the chemicals (including PFAS) and solvents were of reagent grade or above, and used as received from the commercial suppliers. Ultrapure Milli-Q deionized (DI) water was used for all experiments. Synthesis and structural characterization of the fluorophores (**PDI-2+**, **PDI-Cl-2+**, **PDI-6+**) are provided in detail in the supporting information.

NMR data were recorded on a Varian Mercury 400 MHz spectrometer. A Bruker maXis II ETD instrument was used to obtain high resolution ESI MS data. The fluorescence measurements were carried out with an Agilent Cary Eclipse fluorescence spectrophotometer. UV-Vis spectra were obtained by using an Agilent Cary 100 spectrophotometer. Scanning electron microscopy (SEM) images were obtained with a FEI Nova Nano-SEM™ scanning electron microscope.

2.2. Sensor testing and verification

Stock solutions of PDI sensors and all other analytes, viz., perfluorooctanesulfonate (PFOS) potassium salt, perfluorooctanoic acid (PFOA), GenX, sodium dodecyl sulfate (SDS), ethylenediaminetetraacetic acid (EDTA), lauryl sulfate, lauric acid, octanoic acid, trifluoroacetic acid (TFA), sodium chloride (NaCl), potassium chloride (KCl), lithium chloride (LiCl), ferric chloride (FeCl₃), calcium sulfate (CaSO₄), magnesium sulfate (MgSO₄), sodium bicarbonate (NaHCO₃), sodium thiosulfate (Na₂S₂O₃), sodium phosphate (Na₃PO₄) and sodium nitrate (NaNO₃) were prepared at concentrations of 1 mM in DI water. The absorption and fluorescence studies were performed after making different solutions of the sensor molecule (2 μM, or 100 nM) in DI water, each containing various concentrations of each analyte (0–8 μM, or 0–100 nM) in a quartz or polystyrene cuvette (1 cm × 1 cm). Given the strong adherence of PFOS to the cuvette surface, special care must be taken during the preparation of solution samples. For example, a large volume of the fluorophore solution should be poured into a cuvette pre-deposited with a small volume (<10 μL) of concentrated PFOS, followed by thorough mixing. This approach minimizes surface trapping of PFOS, a phenomenon that has been observed and is particularly critical for quantitative sensor analysis involving PFOS, especially in the low

concentration range (e.g., 100 nM). The spectra of each resultant mixture were recorded after mixing the solutions thoroughly at room temperature. The initial emission intensity in the absence of analyte was termed as I_0 . The fluorescence quenching efficiency (Q) was estimated by using the formula: $Q = (1 - I/I_0) \times 100\%$, where I is the emission intensity of the sensor in the presence of analyte.

2.3. Detection of PFOS in real water samples

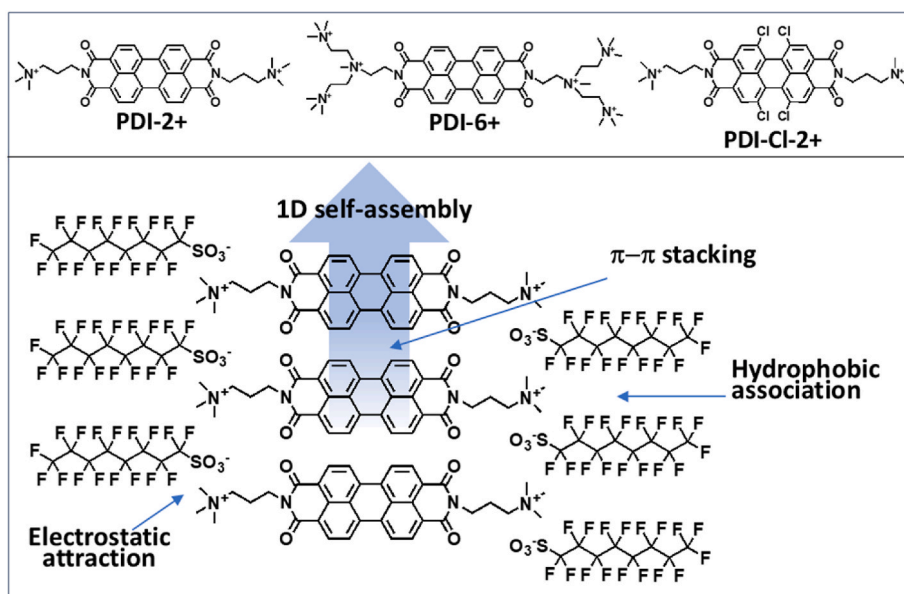
Tap water and drinking water samples were collected from the University of Utah campus and directly used as solvents to prepare spiked PFOS solutions at concentrations of 40 μM and 80 μM. To these solutions, 100 nM of **PDI-2+** was added by diluting a stock solution prepared in DI water. Each solution was prepared to a total fixed volume of 3 mL, suitable for fluorescence measurements using a standard cuvette. All samples were incubated for 1 min prior to fluorescence measurement.

2.4. Quantum yield calculation

The fluorescence quantum yield of the cationic PDI sensors was evaluated by the Parker-Rees method using Rhodamine 6G as a standard fluorophore. The Parker-Rees equation can be written as follows [40].

$$\Phi_u = (A_s F_u n_u^2 / A_u F_s n_s^2) \Phi_s \quad (1)$$

Where Φ_s represents the quantum yield of the reference compound (Rhodamine 6G, with a value of 0.95) and Φ_u denotes the quantum yield of the PDI sensors. A_s and A_u represent the absorbances of Rhodamine 6G and the sensor molecule samples at the excitation wavelength, respectively. To reduce the reabsorption of emitted fluorescence light as it passes through the samples, the absorbance maxima were kept below 0.1. F_s and F_u refer to the integrated fluorescence intensity areas of Rhodamine 6G and the PDI sensor samples, respectively, when excited at the same wavelength. The refractive indices of the solvents used for the PDI sensor samples and Rhodamine 6G are denoted as n_u and n_s , respectively.



Scheme 1. (Top panel) Chemical structures of fluorophores **PDI-2+** and **PDI-6+**. A non-planar PDI analogue, **PDI-Cl-2+**, was synthesized and used for comparative study. (Lower panel) Schematic illustration of the supramolecular complexation between PFOS and **PDI-2+** (2:1 M ratio) leading to 1D self-assembly, and quenching of the fluorescence of PDI.

3. Results and discussion

3.1. Spectral and structural characterization of fluorophores

Three PDI sensors containing quaternized amines groups were designed and synthesized in this study (Scheme 1). Perylene-tetracarboxylic dianhydride (PTCDA) was used as starting material for synthesizing **PDI-2+** and **PDI-6+** [41,42], which contains two and six quaternized amines, respectively. Details of the synthesis and structural characterization of these two compounds can be found in the supporting information (Figs. S1–6). The synthesis of **PDI-Cl-2+** was carried out using the same method as for **PDI-2+**, but with 1,6,7,12-tetrachloro-substituted PTCDA as the precursor instead (Figs. S7–9). **PDI-Cl-2+** was designed and employed for assessing the effect of non-planar structure of PDI on the sensing performance. While the non-substituted PDI is perfectly planar, the tetrachloro-substitution alters it to a tilted conformation with a dihedral angle of ca. 36° [43]. The tilted conformation introduces additional steric hindrance to π - π stacking between PDI planes, which is expected to result in a weakened fluorescence quenching response toward PFOS, as illustrated in Scheme 1. All the three sensor molecules and the synthetic intermediates were characterized by their structure with ^1H NMR and MS spectra (Figs. S1–9).

Due to their cationic nature, all the three fluorophores exhibit good water solubility and produce bright emission. High water solubility is crucial for sensors intended for use in entirely aquatic environments. The introduction of multiple quaternary ammonium groups effectively increases the overall hydrophilicity of the PDI molecule, ensuring better dispersion in water. Furthermore, this charged nature minimizes aggregation by introducing electrostatic repulsion between the side groups, countering the π - π stacking interactions that typically lead to aggregation. Additionally, introducing steric hindrance through bulky substituents at the bay positions, as seen with the chloro groups in **PDI-Cl-2+**, can help to disrupt π - π stacking interactions. These modifications not only enhance solubility but also stabilize the molecular dispersion state in aqueous environments, which is crucial for achieving optimal sensor performance. Initially, we examined the absorption and fluorescence spectra of the three fluorophores in pure water (Fig. S10). The bay-substituted **PDI-Cl-2+** shows three absorption peaks at 524, 490 and 431 nm, which correspond to the $0 \rightarrow 0$, $0 \rightarrow 1$ and $0 \rightarrow 2$ vibronic level of π - π electronic transition, respectively [44–47]. The absorption spectral pattern is characteristic of the molecular dispersion state with the $0 \rightarrow 0$ absorption (524 nm) being the maximum. On the other hand, the non-substituted **PDI-2+** and **PDI-6+** demonstrate absorption maxima at the $0 \rightarrow 1$ transition around 500 nm, implying a tendency towards aggregation induced by π - π stacking [48]. This aggregation leads to significant fluorescence quenching, a phenomenon known as aggregation-induced quenching (AIQ). As a result, the fluorescence quantum yields of **PDI-2+** and **PDI-6+** were found to be notably low, at only 11 % and 15 %, respectively. This is conducive to enhancing the fluorescence quenching efficiency, which is essential for achieving high sensing sensitivity. In contrast, the bay-substituted **PDI-Cl-2+** demonstrated a fluorescence quantum yield as high as 60 %, attributed to the introduction of chloro-substituents at the bay positions. These substitutions introduce a twisted perylene core, effectively reducing π - π stacking and minimizing aggregation. Both **PDI-2+** and **PDI-6+** display a structure-resolved fluorescence spectra with emission maxima around 547 nm, while **PDI-Cl-2+** exhibits a spectrum with significant loss of the vibronic structures. The introduction of four chloro-substitutions at the bay position results in a significantly twisted perylene core in **PDI-Cl-2+**, leading to a less pronounced geometric relaxation upon photoexcitation [49].

3.2. Sensing responses towards PFOS

It is hypothesized that PFOS with anionic head can interact strongly

with cationic fluorophore. Such electrostatic interaction will lead to formation of nanoaggregates, resulting in fluorescence quenching. Here, the three PDI based fluorophores were employed to check the effect of both cationic head group and planarity of the PDI core on the sensing performance. The sensor probe with six quaternized amines (**PDI-6+**) is anticipated to interact more strongly with PFOS than the probe with two quaternized amines (**PDI-2+**). However, it is also suggested that the large, crowded structure and high charge density of **PDI-6+** could prevent effective aggregation upon binding with PFOS.

To evaluate their utility for PFOS sensing, the fluorescence spectra of all three cationic fluorophores (2 μM) were recorded in aqueous solutions containing varying concentrations of PFOS. A low concentration of PDI-based fluorophores was selected to minimize the risk of reabsorption of excitation light by the fluorophore itself, a phenomenon known as the inner filter effect (IFE). Moreover, all the analytes (including both PFAS and interferents) have no absorption at the excitation wavelength, excluding the IFE effect. Before conducting the sensing experiments, the stability of the cationic fluorophores was tested to identify any time-dependent aggregation-induced quenching behavior. As shown in Figs. S11–13, all three probes maintained stable fluorescence for at least 20 min, providing a sufficient time frame to conduct the sensor test. This result confirms the consistent emission behavior and stability of the cationic sensor probes, ensuring their reliability for sensing applications. With an increasing concentration of PFOS from 0 to 6 μM , the emission intensity of **PDI-2+** was drastically quenched up to 98 % (Fig. 1). The **PDI-6+** fluorophore demonstrated a lower quenching efficiency of 70 % under the same conditions (Fig. S14). Clearly, an increased density of cationic charges does not improve but rather slightly decreases the sensing sensitivity of **PDI-6+**, likely due to the compensating electrostatic repulsion between the crowded cationic groups, as discussed above. Under the same testing conditions, the bay-substituted **PDI-Cl-2+** probe shows only 38 % fluorescence quenching (Fig. S15), implying that the planarity of the PDI core is critical for achieving effective π - π stacking and, consequently, fluorescence quenching. Based on these results, it can be concluded that the competitive balance between the electrostatic interactions and π - π stacking plays a crucial role in determining the ultimate sensing performance.

With the **PDI-2+** sensor proven to be the most sensitive, the supramolecular complexation (aggregation) between this fluorophore and PFOS was further characterized by the UV-vis absorption spectrometry,

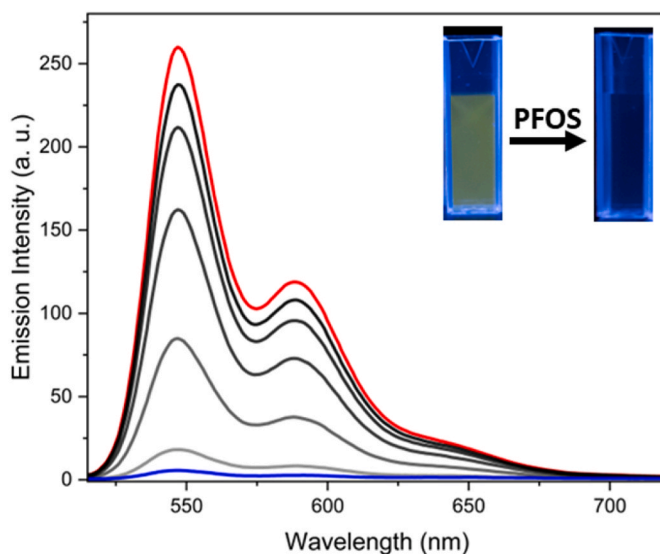


Fig. 1. Fluorescence spectra of **PDI-2+** (2.0 μM) measured in the presence of increasing concentrations (0–6 μM) of PFOS in DI water showing significant emission quenching. Inset: photograph of the solution before and after addition of 6 μM of PFOS taken under 365 nm UV light.

as shown in Fig. 2. With increasing concentrations of PFOS, the absorption peaks of **PDI-2+** at 500 nm and 536 nm, corresponding to the $0 \rightarrow 1$ and $0 \rightarrow 0$ transitions respectively, rapidly decreased and eventually disappeared as the PFOS concentration increased further. Meanwhile, absorption in the shorter wavelength region showed a relative increase. These observations are characteristic of the aggregation behavior of planar PDI fluorophores, similar to what has been observed with other PDI molecules [47,48,50,51]. More interestingly, two isosbestic points were observed at 463 and 585 nm, further indicating the quantitative conversion of the free molecular form of **PDI-2+** to an aggregated state in complexation with PFOS. In comparison, when tested with PFOS under the same conditions, **PDI-6+** exhibited only a slight relative decrease in the $0 \rightarrow 0$ absorption, along with a slight increase at shorter wavelengths, despite a significant overall decrease in absorption due to PFOS-induced aggregation (Fig. S16). This suggests weak or distorted π - π stacking due to steric hindrance from the bulky side chains. For the **PDI-Cl-2+** probe, although the overall absorption decreased, no significant change in the spectral shape was observed (Fig. S17), consistent with the tilted PDI backbone that hinders effective π - π stacking. These spectral changes observed align with the fluorescence quenching obtained for the three fluorophores, with quenching efficiencies in the order of **PDI-2+** > **PDI-6+** > **PDI-Cl-2+**.

The limit of detection (LOD) for PFOS in water media is crucial for evaluating new sensor development. To determine the LOD for the new fluorophores, fluorescence titration experiments were conducted using **PDI-2+** at lower concentration (100 nM) with PFOS added in the concentration range of 0–100 nM. The emission intensity, measured at the maximum wavelength (547 nm), was plotted against the concentration of PFOS (Fig. 3). A linear fluorescence response was observed at lower PFOS concentrations. From the resulting linear calibration curve, a LOD of 3.5 nM (1.9 ppb) was estimated for the **PDI-2+** probe using the IUPAC 3σ criterion. This LOD is superior to that of most fluorescent sensors recently reported for PFOS detection (Table S1). In addition to its high sensitivity, **PDI-2+** also demonstrates exceptional selectivity towards PFOS, particularly over PFOA, as described later. This makes **PDI-2+** an ideal candidate for practical, portable sensor applications. Very few, if any, fluorescent sensors reported to date can match the combined high sensitivity and selectivity exhibited by **PDI-2+** (Table S1). A similar fluorescence quenching titration was performed for **PDI-6+**, yielding an

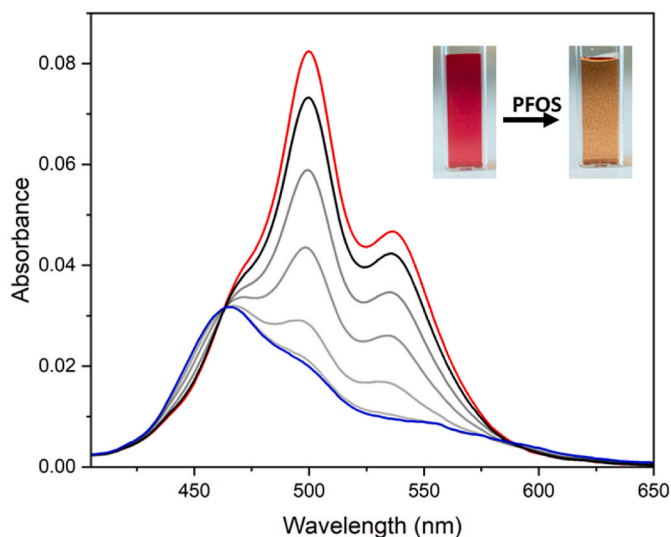


Fig. 2. UV-vis absorption spectra of **PDI-2+** (2.0 μ M) in the presence of increasing concentrations of PFOS (0–6 μ M, red to blue) in DI water. Inset: photograph of **PDI-2+** solution (0.1 mM) before and after addition of 0.3 mM of PFOS taken under day light, for which high concentration was used in order to reveal clearly the color change. (For interpretation of the references to color in this figure legend, the reader is referred to the Web version of this article.)

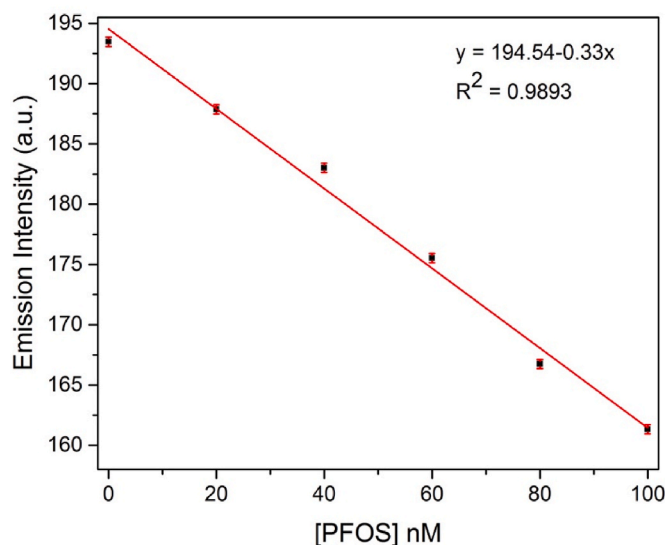


Fig. 3. Change in the emission intensity of **PDI-2+** (100 nM) as a function of PFOS concentration in DI water.

LOD of 2.7 nM (1.4 ppb) within the same concentration range of 0–100 nM (Fig. S18). The slightly improved LOD observed for **PDI-6+**, despite its marginally lower quenching efficiency, is primarily attributed to its enhanced solubility and dispersibility in water compared to **PDI-2+**. This improved solubility stabilizes the fluorescence intensity measurements, resulting in reduced standard deviations.

To assess the selectivity of **PDI-2+** for PFOS, other PFAS compounds (e.g., PFOA, GenX), along with a broad range of common chemicals—including surfactants (e.g., SDS), acids (e.g., trifluoroacetic acid, Lauric acid, Octanoic acid), cosmetic components (e.g., EDTA, Lauryl sulfate), and metal salts (e.g., NaCl, KCl, LiCl, FeCl₃, CaSO₄, MgSO₄, NaHCO₃, Na₂S₂O₃, Na₃PO₄ and NaNO₃) were tested under the same fluorescence titration conditions used for PFOS. As clearly shown in Fig. 4a and Fig. S19, high selectivity was achieved against all tested interferents, including PFAS analogues. To further verify detection specificity, the fluorescence quenching response towards PFOS was examined in the presence of each interferent, to assess potential cross-reactivity among coexisting analytes. Remarkably, the quenching efficiency of PFOS remained almost unchanged despite the presence of interferents (Fig. 4b, Fig. S20), demonstrating the robustness of the sensor's selectivity. The high selectivity can be attributed to the specific complexation between **PDI-2+** and PFOS, facilitated and reinforced by the synergistic intermolecular interactions illustrated in Scheme 1. A similar trend was observed for **PDI-6+** and PFOS and other competing analytes (Fig. S21).

3.3. Characterization of PFOS induced molecular aggregation

It is essential to explore the details of the molecular aggregation of fluorophore **PDI-2+** induced by PFOS, as this directly correlates with the sensing mechanism. A comprehensive understanding of this mechanism would provide valuable insights that can inform the design of future sensors with enhanced performance in terms of either sensitivity or selectivity. The absorption spectral measurements presented above indicate strong π - π stacking interactions between the planar core of **PDI-2+** in the presence of PFOS. Such columnar stacking arrangement, induced by PFOS, is expected to result in one-dimensional (1D) self-assembly of the molecule (Scheme 1), ultimately leading to the formation of nanofibril structures. As demonstrated by SEM imaging in Fig. 5, well-defined nanofibril structures were indeed formed from **PDI-2+** in the presence of PFOS, wherein the nanofibers appear intertwined, forming a network. Similar nanofibril structures have been reported for

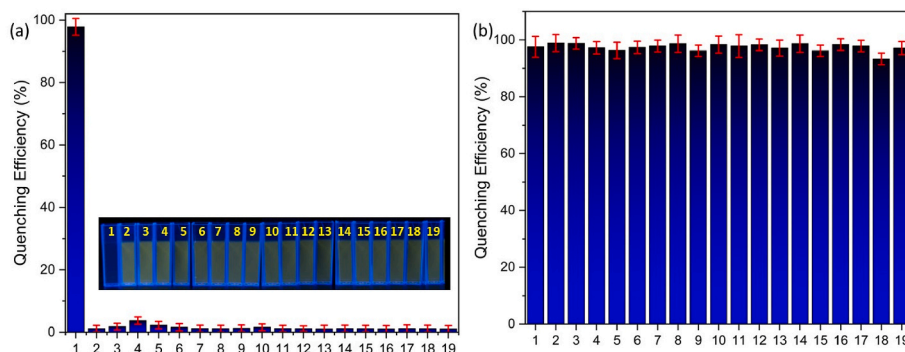


Fig. 4. (a) Fluorescence quenching efficiency of **PDI-2+** (2 μM) towards various analytes; (1) PFOS, (2) PFOA, (3) GenX, (4) SDS, (5) EDTA, (6) Lauryl Sulfate, (7) Lauric Acid, (8) TFA, (9) n-octanoic acid, (10) Na^+ , (11) K^+ , (12) Li^+ , (13) Ca^{2+} , (14) Mg^{2+} , (15) Fe^{3+} , (16) $\text{S}_2\text{O}_3^{2-}$, (17) HCO_3^- , (18) PO_4^{3-} and (19) NO_3^- (all at 6 μM). Inset: photograph **PDI-2+** solutions in the presence of the 19 analytes under UV light. (b) Fluorescence quenching efficiency of **PDI-2+** by PFOA co-present with different interfering analytes: (1) no interfering analyte, (2) PFOA, (3) GenX, (4) SDS, (5) EDTA, (6) Lauryl Sulfate, (7) Lauric Acid, (8) TFA, (9) n-octanoic acid, (10) Na^+ , (11) K^+ , (12) Li^+ , (13) Ca^{2+} , (14) Mg^{2+} , (15) Fe^{3+} , (16) $\text{S}_2\text{O}_3^{2-}$, (17) HCO_3^- , (18) PO_4^{3-} and (19) NO_3^- (each at 6 μM).

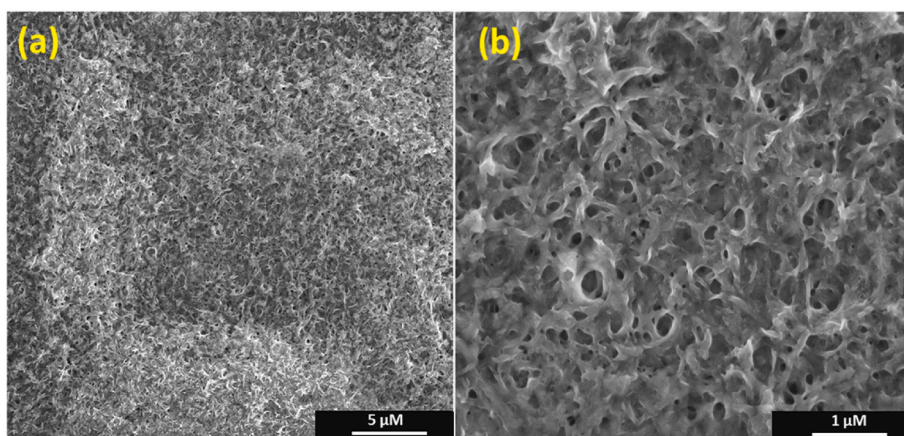


Fig. 5. (a) and (b) SEM images of the **PDI-2+** /PFOS nanofibril network with different magnifications.

many other PDI molecules that undergo 1D self-assembly in solution, also primarily driven by π - π stacking interactions [37,52–55].

As illustrated in Scheme 1, the stacking assembly of **PDI-2+** is enabled and facilitated by its association of PFOS. The cationic nature of **PDI-2+** would typically hinder tight cofacial stacking (and thus prevent 1D growth of the assembly) due to electrostatic repulsion between the molecules. Indeed, when tested under the same conditions but without PFOS, **PDI-2+** only formed irregular particulate aggregates, with no fibril structures observed (Fig. S22). The association with anionic PFOS not only neutralizes the cationic charge of **PDI-2+**, but also reinforces the intermolecular arrangement through hydrophobic interactions between the long fluorinated alkyl chains. As characterized with Job's plot (Fig. S23), the association between **PDI-2+** and PFOS follows a 1:2 M

ratio, aligning with the charge ratio of the two molecules, satisfying charge neutrality. Similar to the findings of this study, the binding-induced assembly of PDI fluorophores has previously been utilized to develop sensors for detecting various types of chemicals and ions [38, 56–59].

The supramolecular complexation between **PDI-2+** and PFOS was further characterized using ^1H NMR spectrometry, providing detailed structural insights into the intermolecular interactions and aggregation of **PDI-2+** induced by PFOS. As shown in Fig. 6, with increasing concentrations of PFOS, the ^1H NMR peaks for all protons of **PDI-2+** (including both the core and side chain) decrease significantly in intensity, indicative of an aggregated state. Along with the reduction in intensity, a distinct upfield shift is observed in the perylene proton peaks

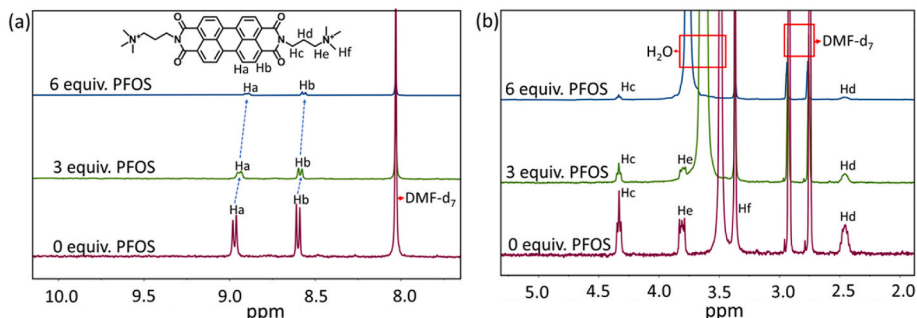


Fig. 6. Change in ^1H NMR spectrum of **PDI-2+** in the presence of increasing concentrations of PFOS as highlighted for the aromatic (a) and aliphatic (b) region.

(Fig. 6a), attributed to the shielding effects of the perylene core due to π - π stacking [60,61]. In contrast, no shift is observed for the protons within the aliphatic side-chain of PDI-2+ (Fig. 6b), suggesting that there is no significant change in shielding after the original counterion Γ^- is replaced by the sulfonate ion ($-\text{SO}_3^-$) during complexation with PFOS.

3.4. Detection of PFOS in real water samples

An ideal sensor must work in real life complex environment. The linear calibration curve obtained (Fig. 3) can be used to quantify the unknown concentration of PFOS. The real water samples such as tap and drinking water were used to evaluate the capabilities of the current sensor in complex matrices. To verify this hypothesis, PFOS was spiked into one drinking water sample and two tap water samples at concentrations of 40 and 80 nM, followed by the addition of 100 nM PDI-2+. Fluorescence measurements of the solutions, compared to those without PFOS, yielded quenching efficiencies, which were then used to calculate the concentration by referencing the calibration curve. The estimated concentration was compared to the actual spiked concentration to assess the sensor's detection accuracy. As summarized in Table S2, good recovery rates between 103 % and 107 % were obtained for all the real water samples. These results suggest the high feasibility of using PDI-2+ for precise aqueous detection of PFOS in practical applications. Furthermore, given that the pH of real water samples may vary depending on their constituents, an effective sensor must perform reliably across a wide pH range. When tested with a fixed concentration of PFOS in water (6 μM), both PDI-2+ and PDI-6+ sensors demonstrated consistent fluorescence quenching over a pH range of 3–11 (Fig. S24). These findings further underscore the potential of PDI sensors for effective PFOS detection in real-world water samples.

4. Conclusions

In summary, we have developed an effective fluorescent sensor for detecting PFOS in water solutions with high sensitivity and selectivity. The sensor is based on a PDI molecule modified with cationic side groups at both imide positions. Under optimal conditions, the limit of detection (LOD) can reach as low as 3.5 nM (or 1.9 ppb) and 2.7 nM (1.4 ppb), as determined for PDI-2+ and PDI-6+, respectively. The sensor has been validated across various water samples, including tap and drinking water, providing precise detection of PFOS. The sensor operates in a fluorescence quenching mode, caused by the molecular aggregation induced by complexation with PFOS. This complexation and subsequent aggregation, as characterized through comprehensive spectroscopy and microscopy techniques, result from a synergistic interplay of multiple interactions between the fluorophore and PFOS, including electrostatic attraction, π - π stacking, and hydrophobic association. This sensor technology holds great potential for rapid and onsite PFOS detection or monitoring, offering advantages such as a fast response, high sensitivity, excellent selectivity, water solubility, user-friendliness, and cost-effectiveness. The structural design and optimization strategies outlined in this study are versatile and can be further adapted to develop novel fluorophores for detecting other PFAS compounds, thereby contributing to enhanced environmental and public health risk assessment and monitoring efforts.

CRediT authorship contribution statement

Rana Dalapati: Writing – original draft, Formal analysis, Data curation. **Saravanakumar Manickam:** Formal analysis, Data curation. **Jiangfan Shi:** Investigation, Formal analysis, Data curation. **Matthew Hunter:** Writing – review & editing, Data curation. **Ling Zang:** Writing – review & editing, Visualization, Supervision, Resources, Project administration, Funding acquisition, Conceptualization.

Declaration of competing interest

Ling Zang has a significant financial interest in Gentex Corporation, which funded this research.

Acknowledgements

The authors are grateful to Gentex Corporation for research sponsorship, and the University of Utah for instrumental facilities and other support. This work was sponsored by Gentex Corporation under award #10060686, and University of Utah Ascender project (#51900526).

Appendix A. Supplementary data

Supplementary data to this article can be found online at <https://doi.org/10.1016/j.aca.2025.343670>.

Data availability

Data will be made available on request.

References

- [1] J. Glüge, M. Scheringer, I.T. Cousins, J.C. DeWitt, G. Goldenman, D. Herzke, R. Lohmann, C.A. Ng, X. Trier, Z. Wang, An overview of the uses of per- and polyfluoroalkyl substances (PFAS), *Environ. Sci.: Processes Impacts* 22 (2020) 2345–2373, <https://doi.org/10.1039/D0EM00291G>.
- [2] C. Ng, I.T. Cousins, J.C. DeWitt, J. Glüge, G. Goldenman, D. Herzke, R. Lohmann, M. Miller, S. Patton, M. Scheringer, X. Trier, Z. Wang, Addressing urgent questions for PFAS in the 21st century, *Environ. Sci. Technol.* 55 (2021) 12755–12765, <https://doi.org/10.1021/acs.est.1c03386>.
- [3] What we know: per- and polyfluoroalkyl substances (PFAS) AAAS center for scientific evidence in public issues. <https://www.aaas.org/programs/epi-center/what-we-know-about-pfas>, 2022, 1st October 2024.
- [4] B.E. Blake, S.E. Fenton, Early life exposure to per- and polyfluoroalkyl substances (PFAS) and latent health outcomes: a review including the placenta as a target tissue and possible driver of peri- and postnatal effects, *Toxicology* 443 (2020) 152565, <https://doi.org/10.1016/j.tox.2020.152565>.
- [5] C. Hogue, US drinking water to be tested for 29 PFAS, *Chemical & Engineering News*, 2021. <https://cen.acs.org/environment/persistent-pollutants/US-drinking-water-tested-29/99/web/2021/12>. (Accessed 1 October 2024).
- [6] C. Hogue, EPA sets health advisory levels for 6 PFAS, *C&EN Global Enterprise*, 2022. <https://pubs.acs.org/doi/10.1021/cen-10022-polcon2>. (Accessed 29 December 2024).
- [7] The US EPA website of safe drinking water Act (SDWA), Last updated on July 14 2022, <https://www.epa.gov/sdwa>, <https://cen.acs.org/environment/persistent-pollutants/US-EPA-sets-health-advisory-6-PFAS/100/i22>. (Accessed 1 October 2024).
- [8] C. Ng, I.T. Cousins, J.C. DeWitt, J. Glüge, G. Goldenman, D. Herzke, R. Lohmann, M. Miller, S. Patton, M. Scheringer, Addressing urgent questions for PFAS in the 21st Century, *Environ. Sci. Technol.* 55 (2021) 12755–12765, <https://doi.org/10.1021/acs.est.1c03386>.
- [9] R.F. Menger, E. Funk, C.S. Henry, T. Borch, Sensors for detecting per- and polyfluoroalkyl substances (PFAS): a critical review of development challenges, current sensors, and commercialization obstacles, *Chem. Eng. J.* 417 (2021) 129133, <https://doi.org/10.1016/j.cej.2021.129133>.
- [10] R. Li, S. Alomari, R. Stanton, M.C. Wasson, T. Islamoglu, O.K. Farha, T.M. Holsen, S.M. Thagard, D.J. Trivedi, M. Wriedt, Efficient removal of per- and polyfluoroalkyl substances from water with zirconium-based metal-organic frameworks, *Chem. Mater.* 33 (2021) 3276–3285, <https://doi.org/10.1021/acs.chemmater.1c00324>.
- [11] Y. Wang, S.B. Darling, J. Chen, Selectivity of per- and polyfluoroalkyl substance sensors and sorbents in water, *ACS Appl. Mater. Interfaces* 13 (2021) 60789–60814, <https://doi.org/10.1021/acsami.1c16517>.
- [12] T.A. Berthold, A. McCrary, S. deVilleneuve, M. Schramm, Let's talk about PFAS: inconsistent public awareness about PFAS and its sources in the United States, *PLoS One* 18 (2023) e0294134, <https://doi.org/10.1371/journal.pone.0294134>.
- [13] H. Chen, X. Guan, Q. Liu, L. Yang, J. Guo, F. Gao, Y. Qi, X. Wu, F. Zhang, X. Tian, Co-Assembled nanocarriers of de novo thiol-activated hydrogen sulfide donors with an RGDFP pentapeptide for targeted therapy of non-small-cell lung cancer, *ACS Appl. Mater. Interfaces* 14 (2022) 53475–53490, <https://doi.org/10.1021/acsami.2c14570>.
- [14] The US EPA, Biden-harris administration finalizes critical rule to clean up PFAS contamination to protect public health. <https://www.epa.gov/newsreleases/biden-harris-administration-finalizes-critical-rule-clean-pfas-contamination-protect>, 2024, 1st October 2024.
- [15] H. Ryu, B. Li, S. De Guise, J. McCutcheon, Y. Lei, Recent progress in the detection of emerging contaminants PFASs, *J. Hazard Mater.* 408 (2021) 124437, <https://doi.org/10.1016/j.jhazmat.2020.124437>.

- [16] F. Caroleo, G. Magna, M.L. Naitana, L. Di Zazzo, R. Martini, F. Pizzoli, M. Muduganti, L. Lvova, F. Mandoj, S. Nardis, M. Stefanelli, C. Di Natale, R. Paollesse, Advances in optical sensors for persistent organic pollutant environmental monitoring, *Sensors* 22 (2022) 2649, <https://doi.org/10.3390/s22072649>.
- [17] M. Al Amin, Z. Sobhani, Y. Liu, R. Dharmaraja, S. Chadalavada, R. Naidu, J. M. Chalker, C. Fang, Recent advances in the analysis of per- and polyfluoroalkyl substances (PFAS)—a review, *Environ. Technol. Innovat.* 19 (2020) 100879, <https://doi.org/10.1016/j.eti.2020.100879>.
- [18] The US EPA, Method 1633: analysis of per- and polyfluoroalkyl substances (PFAS) in aqueous, solid, biosolids, and tissue samples by LC-MS/MS, chrome-extension://efaidnbmnnnibpcajpcglclefindmkaj/<https://www.epa.gov/system/files/documents/2024-01/method-1633-final-for-web-posting.pdf>, 2022, 1st October 2024.
- [19] R. Khan, Z.O. Uygun, D. Andreescu, S. Andreescu, Sensitive detection of perfluoroalkyl substances using MXene-AgNP-based electrochemical sensors, *ACS Sens.* 9 (2024) 3403–3412, <https://doi.org/10.1021/acssensors.4c00776>.
- [20] R.F. Menger, J.J. Beck, T. Borch, C.S. Henry, Colorimetric paper-based analytical device for perfluorooctanesulfonate detection, *ACS ES&T Water* 2 (2022) 565–572, <https://doi.org/10.1021/acsestwater.1c00356>.
- [21] K.L. Rodriguez, J.-H. Hwang, A.R. Eshfahani, A.H. Sadmani, W.H. Lee, Recent developments of PFAS-detecting sensors and future direction: a review, *Micromachines* 11 (2020) 667, <https://doi.org/10.3390/mi11070667>.
- [22] Q. Zhang, M. Liao, K. Xiao, K. Zhuang, W. Zheng, Z. Yao, A water-soluble fluorescence probe based on perylene diimide for rapid and selective detection of perfluorooctane sulfonate in 100% aqueous media, *Sensor. Actuator. B Chem.* 350 (2022) 130851, <https://doi.org/10.1016/j.snb.2021.130851>.
- [23] R. Dalapati, M. Hunter, M. Sk, X. Yang, L. Zang, Fluorescence turn-on detection of perfluorooctanoic acid (PFOA) by perylene diimide-based metal-organic framework, *ACS Appl. Mater. Interfaces* 16 (2024) 32344–32356, <https://doi.org/10.1021/acami.4c03389>.
- [24] B. Chen, Z. Yang, X. Qu, S. Zheng, D. Yin, H. Fu, Screening and discrimination of perfluoroalkyl substances in aqueous solution using a luminescent metal-organic framework sensor array, *ACS Appl. Mater. Interfaces* 13 (2021) 47706–47716, <https://doi.org/10.1021/acami.1c15528>.
- [25] Y. Luo, S. Ma, J. Zhang, Q. Zhang, Y. Zhang, J. Mao, H. Yuan, G. Ouyang, S. Zhang, W. Zhao, Developing a novel strategy for fabricating matrix film to assess the distribution of potassium perfluorooctanoic sulfonate by matrix-assisted laser desorption/ionization mass spectrometry imaging, *Anal. Chim. Acta* 1303 (2024) 342528, <https://doi.org/10.1016/j.aca.2024.342528>.
- [26] H. Li, Y. Peng, X. Huang, R. Wan, L. Zhang, X. Wang, L. Han, L. Li, C. Wang, J. Chen, Advances in design and preparation of nanozymes and their applications for constructing higher sensitive lateral flow assays, *Coord. Chem. Rev.* 510 (2024) 215797, <https://doi.org/10.1016/j.ccr.2024.215797>.
- [27] C.M. Taylor, M.C. Breadmore, N.L. Kilah, Colorimetric determination of perfluorocarboxylic acids using porphyrin hosts and mobile phone photographs, *Sens. Diagn.* 2 (2023) 676–686, <https://doi.org/10.1039/D3SD00035D>.
- [28] M.H. Hassan, R. Khan, D. Andreescu, S. Shrestha, M. Cotlet, S. Andreescu, Atomically precise hexanuclear Ce (IV) clusters as functional fluorescent nanosensors for rapid one-step detection of PFAS, *Adv. Funct. Mater.* (2024) 2403364, <https://doi.org/10.1002/adfm.202403364>.
- [29] W. Li, G.S. Kaminski Schierle, B. Lei, Y. Liu, C.F. Kaminski, Fluorescent nanoparticles for super-resolution imaging, *Chem. Rev.* 122 (2022) 12495–12543, <https://doi.org/10.1021/acs.chemrev.2c00050>.
- [30] R.B. Clark, J.E. Dick, Electrochemical sensing of perfluorooctanesulfonate (PFOS) using ambient oxygen in river water, *ACS Sens.* 5 (2020) 3591–3598, <https://doi.org/10.1021/acssensors.0c01894>.
- [31] R. Kazemi, E.I. Potts, J.E. Dick, Quantifying interferent effects on molecularly imprinted polymer sensors for per- and polyfluoroalkyl substances (PFAS), *Anal. Chem.* 92 (2020) 10597–10605, <https://doi.org/10.1021/acs.analchem.0c01565>.
- [32] Y.H. Cheng, D. Barpaga, J.A. Soltis, V. Shuthanandan, R. Kargupta, K.S. Han, B. P. McGrail, R.K. Motkuri, S. Basuray, S. Chatterjee, Metal-organic framework-based microfluidic impedance sensor platform for ultrasensitive detection of perfluorooctanesulfonate, *ACS Appl. Mater. Interfaces* 12 (2020) 10503–10514, <https://doi.org/10.1021/acami.9b22445>.
- [33] N. Karimian, A.M. Stortini, L.M. Moretto, C. Costantino, S. Bogialli, P. Ugo, Electrochemosensor for trace analysis of perfluorooctanesulfonate in water based on a molecularly imprinted poly(o-phenylenediamine) polymer, *ACS Sens.* 3 (2018) 1291–1298, <https://doi.org/10.1021/acssensors.8b00154>.
- [34] M.W. Glasscott, K.J. Vannoy, R. Kazemi, M.D. Verber, J.E. Dick, μ -MIP: molecularly imprinted polymer-modified microelectrodes for the ultrasensitive quantification of GenX (HFPO-DA) in river water, *Environ. Sci. Technol. Lett.* 7 (2020) 489–495, <https://doi.org/10.1021/acs.estlett.0c0034>.
- [35] M.B. Garada, B. Kabagambe, Y. Kim, S. Amemiya, Ion-transfer voltammetry of perfluoroalkanesulfonates and perfluoroalkane-carboxylates: picomolar detection limit and high lipophilicity, *Anal. Chem.* 86 (2014) 11230–11237, <https://doi.org/10.1021/ac5027836>.
- [36] R. Ranaweera, C. Ghafari, L. Luo, Bubble-nucleation-based method for the selective and sensitive electrochemical detection of surfactants, *Anal. Chem.* 91 (2019) 7744–7748, <https://doi.org/10.1021/acs.analchem.9b01060>.
- [37] S. Chen, P. Slattum, C. Wang, L. Zang, Self-assembly of perylene imide molecules into 1D nanostructures: methods, morphologies, and applications, *Chem. Rev.* 115 (2015) 11967–11998, <https://doi.org/10.1021/acs.chemrev.5b00312>.
- [38] J. Wu, M. Peng, M. Mu, J. Li, M. Yin, Perylene diimide supramolecular aggregates: constructions and sensing applications, *Supramol. Mater.* 2 (2023) 100031, <https://doi.org/10.1016/j.supmat.2023.100031>.
- [39] M. Gledhill, A.J. Beck, B. Stamer, C. Schlosser, E.P. Achterberg, Quantification of munition compounds in the marine environment by solid phase extraction–ultra high performance liquid chromatography with detection by electrospray ionisation–mass spectrometry, *Talanta* 200 (2019) 366–372, <https://doi.org/10.1016/j.talanta.2019.03.050>.
- [40] L. Gao, R. Dalapati, B. Gao, X. Huang, D. Zhao, F. Wang, L. Zang, Mitochondrial STED imaging and membrane potential monitoring with a cationic molecular probe, *Small Methods* 8 (2024) 2400525, <https://doi.org/10.1002/smt.202400525>.
- [41] T. Ma, C. Li, G. Shi, Optically active supramolecular complex formed by ionic self-assembly of cationic perylene diimide derivative and adenosine triphosphate, *Langmuir* 24 (2008) 43–48, <https://doi.org/10.1021/la702559m>.
- [42] Z. Xu, W. Cheng, K. Guo, J. Yu, J. Shen, J. Tang, W. Yang, M. Yin, Molecular size, shape, and electric charges: essential for perylene bisimide-based DNA intercalator to localize in cell nuclei and inhibit cancer cell growth, *ACS Appl. Mater. Interfaces* 7 (2015) 9784–9791, <https://doi.org/10.1021/acsami.5b01665>.
- [43] Z. Chen, M.G. Debije, T. Dabaerdemaker, P. Osswald, F. Würthner, Tetrachloro-substituted perylene bisimide dyes as promising n-type organic semiconductors: studies on structural, electrochemical and charge transport properties, *ChemPhysChem* 5 (2004) 137–140, <https://doi.org/10.1002/cphc.200300882>.
- [44] J. Liu, Y. Zhang, C. Zhang, P. Zhang, R. Zeng, J. Cui, J. Chen, Perylene diimide-based supramolecular polymer with temperature-sensitive ratiometric fluorescence responsiveness in solution and gels, *Mater. Adv.* 1 (2020) 1330–1336, <https://doi.org/10.1039/D0MA00053A>.
- [45] L. Zang, Y. Che, J.S. Moore, One-dimensional self-assembly of planar π -conjugated molecules: adaptable building blocks for organic nanodevices, *Acc. Chem. Res.* 41 (2008) 1596–1608, <https://doi.org/10.1021/ar800030w>.
- [46] K. Balakrishnan, A. Datar, T. Naddo, J. Huang, R. Oitker, M. Yen, J. Zhao, L. Zang, Effect of side-chain substituents on self-assembly of perylene diimide molecules: morphology control, *J. Am. Chem. Soc.* 128 (2006) 7390–7398, <https://doi.org/10.1021/ja061810z>.
- [47] K. Balakrishnan, A. Datar, R. Oitker, H. Chen, J. Zuo, L. Zang, Nanobelt self-assembly from an organic n-type semiconductor: propoxyethyl-PTCDI, *J. Am. Chem. Soc.* 127 (2005) 10496–10497, <https://doi.org/10.1021/ja052940v>.
- [48] A. Datar, K. Balakrishnan, L. Zang, One-dimensional self-assembly of a water soluble perylene diimide molecule by pH triggered hydrogelation, *Chem. Commun.* 49 (2013) 6894–6896, <https://doi.org/10.1039/C3CC43359E>.
- [49] P. Leowanawat, A. Nowak-Król, F. Würthner, Tetramethoxy-bay-substituted perylene bisimides by copper-mediated cross-coupling, *Org. Chem. Front.* 3 (2016) 537–544, <https://doi.org/10.1039/C6QO00047A>.
- [50] R. Dalapati, M. Hunter, L. Zang, A dual fluorometric and colorimetric sulfide sensor based on coordinating self-assembled nanorods: applicable for monitoring meat spoilage, *Chemosensors* 10 (2022) 500, <https://doi.org/10.3390/chemosensors10120500>.
- [51] J. Seo, M.I. Khazi, K. Bae, J.M. Kim, Temperature-controlled pathway complexity in self-assembly of perylene diimide-polydiacetylene supramolecule, *Small* 19 (2023) 2206428, <https://doi.org/10.1002/smll.202206428>.
- [52] F. Zhang, Y. Ma, Y. Chi, H. Yu, Y. Li, T. Jiang, X. Wei, J. Shi, Self-assembly, optical and electrical properties of perylene diimide dyes bearing unsymmetrical substituents at bay position, *Sci. Rep.* 8 (2018) 8208, <https://doi.org/10.1038/s41598-018-26502-5>.
- [53] L. Zang, Y. Che, J.S. Moore, One-dimensional self-assembly of planar π -conjugated molecules: adaptable building blocks for organic nanodevices, *Acc. Chem. Res.* 41 (2008) 1596–1608, <https://doi.org/10.1021/ar800030w>.
- [54] Y. Che, A. Datar, K. Balakrishnan, L. Zang, Ultralong nanobelts self-assembled from an asymmetric perylene tetracarboxylic diimide, *J. Am. Chem. Soc.* 129 (2007) 7234–7235, <https://doi.org/10.1021/ja071903w>.
- [55] M.T. Usowicz, M.J. Kelley, K.D. Singer, V.V. Duzhko, Tailored one-and two-dimensional self-assembly of a perylene diimide derivative in organic solvents, *J. Phys. Chem. B* 115 (2011) 9703–9709, <https://doi.org/10.1021/jp203703e>.
- [56] S. Chen, Z. Xue, N. Gao, X. Yang, L. Zang, Perylene diimide-based fluorescent and colorimetric sensors for environmental detection, *Sensors* 20 (2020) 917, <https://doi.org/10.3390/s20030917>.
- [57] B. Pramanik, S. Das, D. Das, Aggregation-directed high fidelity sensing of picric acid by a perylene diimide-based luminogen, *Chem. Asian J.* 15 (2020) 4291–4296, <https://doi.org/10.1002/asia.202001184>.
- [58] Y. Wu, Q. Zhang, Y. Zhao, K. Zhuang, Y. Fan, S. Zhang, X. Zhang, K. Huang, Z. Yao, A sensitive and selective fluorescent sensor for berberine chloride based on the supramolecular self-assembly of perylene diimide in aqueous solution, *ACS Sustainable Chem. Eng.* 8 (2020) 6517–6523, <https://doi.org/10.1021/acscuschemeng.0c01177>.
- [59] W. Zheng, Y. Zhao, X. Lin, Q. Zhang, K. Xiao, N. Cheng, X. Mei, Y. Lu, Z. Yao, Rapid and selective detection of picric acid based on supramolecular self-assembly of a cationic perylene diimide in pure aqueous media, *Dyes Pigments* 207 (2022) 110761, <https://doi.org/10.1016/j.dyepig.2022.110761>.
- [60] P. Yan, A. Chowdhury, M.W. Holman, D.M. Adams, Self-organized perylene diimide nanofibers, *J. Phys. Chem. B* 109 (2005) 724–730, <https://doi.org/10.1021/jp046133e>.
- [61] D. Wei, L. Ge, Z. Wang, Y. Wang, R. Guo, Self-Assembled dual helical nanofibers of amphiphilic perylene diimides with oligopeptide substitution, *Langmuir* 35 (2019) 11745–11754, <https://doi.org/10.1021/acs.langmuir.9b01745>.